RTM 3D angle gathers for OBN data using an equal area spherical binning method

Roberto Pereira, Ivan Coulamy, Adriano Martinez (CGG); Werter Oliveira, Eduardo Naomitsu (Petrobras)*

Summary

Compared with towed-streamer acquisitions, ocean bottom nodes (OBN) generally provide fuller-azimuth illumination of the subsurface, longer offsets, higher signal-to-noise ratio (S/N), and improved low frequencies. These advantages provide the necessary ingredients for two key elements of seismic exploration and monitoring: (i) full-waveform inversion (FWI) with better constrained velocity models and (ii) imaging below complex structures with improved illumination. In order to take full advantage of this data, it is imperative to use the best imaging algorithm available.

Reverse time migration (RTM) is well suited for imaging deep and complex structures. Moreover, it can be modified to yield angle-domain common-image gathers (ADCIGs). These gathers inherit the usual benefits of RTM, when compared to other imaging algorithms, while providing prestack images with reliable subsurface information. This information can be used for amplitude variation with angle/offset (AVA/O) inversion, migration velocity analysis (MVA), and other prestack domain methods.

We will investigate data sampling issues related to the implementation of RTM 3D angle gathers, which are more prominent in the case of OBN acquisitions, and propose a method for sampling the subsurface reflection energy that better represents the full-azimuth nature of OBN data while honoring the amplitudes of the image gathers.

Introduction

OBN acquisitions often provide the best data for imaging complex areas. The full-azimuth data combined with long offsets and better S/N guarantees improved illumination of the subsurface, as well as better constrained velocity inversion through FWI (Bunting and Moses, 2016), compared to towed-streamer data.

3D ADCIGs generated by RTM are, in principle, the best current solution for imaging in complex regions. They have the usual benefits of RTM when compared to other imaging algorithms, such as Kirchhoff and one-way wave-equation migration (WEM). Additionally, they also produce angle-dependent prestack images of the subsurface. Angle gathers are well-suited to overcome potential issues with surface-based prestack images (Xu et al., 2001), such as migration artifacts caused by multiple ray-paths. Moreover, they generate asymptotically true amplitude images (Xu et al., 2011), making them appropriate for AVA/O inversion (Tura et al., 1998).

One of the challenges faced when implementing RTM angle gathers is their sensitivity to acquisition sampling, as noted by Tang et al. (2011). This issue is accentuated in the case of OBN data (Docherty and Schneider Jr., 2016), given the larger receiver separation commonly used in this type of acquisition. Tang et al. (2011) estimate a variable angular bin size that depends on incident angle, reflector depth, and source separation, which should be replaced by node separation in the OBN case, using reciprocity. Based on that estimation, the authors propose to extrapolate the specular energy at given angle and depth. Docherty and Schneider Jr. (2016) define a mapping to angle domain using band-limited binning functions. On the other hand, Vyas et al. (2011) propose a spherical binning method based on the approximation of the sphere by an icosahedron, following Tegmark (1996).

We propose a different spherical binning method that is suitable for full-azimuth acquisitions and honors the true amplitude nature of the image. Results of this method applied to OBN data from the Santos Basin, offshore Brazil, are presented.

Method

Approaches for constructing 3D angle gathers from RTM can be divided into two main classes of algorithms. One relies on extended images as an intermediate step (e.g., Fomel, 2004) for computing angle gathers. Another class computes the gathers directly by estimating the wavefield directions, e.g., computing Poynting vectors of source and receiver wavefields (Yoon and Marfurt, 2006), using source directions (Vyas et al., 2011), or decomposing wavefields in the wavenumber-frequency domain (Xu et al., 2011). Our proposed binning method can be applied to any algorithm of the second class, where the image is binned directly in the angle domain. It can also be extended in principle to WEM and Kirchhoff migrations.

In order to compute RTM angle gathers, the incident and azimuth reflection angles between the forward and backward wavefields are computed at each point in the image domain. The image obtained by crosscorrelation is then binned in reflection angle, θ, and azimuth, ϕ. Typically, bins are defined in cylindrical coordinates with a window function:

$$W^{cyl}_{\theta^*,\phi^*}(\theta,\phi) \sim \frac{1}{sin\theta^*}\,\delta(\theta-\theta^*)\delta(\phi-\phi^*)\ , \quad (1)$$

where (θ^*,ϕ^*) represents the center of the angle bin. This function appears, for example, in the true-amplitude formula of Xu et al. (2011). The factor of $1/\sin\theta^*$ is present to

compensate for the fact that the bins become smaller as they approach the pole ($\theta^* = 0$).

Regardless of the method used to compute the angles, the choice of binning function W_{θ^*,ϕ^*} affects the overall quality and amplitude behavior of the image gathers. It should be chosen such that it best represents the sampling of reflection energy around the image point, which in turn depends on the data sampling defined by the acquisition. The coarser the data sampling, the more sensitive the results are with respect to the choice of the binning function, which is the case for OBN acquisitions. Indeed, the use of cylindrical coordinates tends to over-sample the near angles while under-sampling the far angles, as shown in Figure 1.

Since the reflection coefficients at a given image point can be given as a function of incident reflection angle and azimuth, it is natural to look for a binning of the sphere parameterized by these two angles. The idea of using an optimal sampling of the sphere for constructing RTM angle gathers has been proposed in Vyas et al. (2011). This method is based on the approximation of the sphere by an icosahedron, following Tegmark (1996), who first introduced it for sampling sky maps in astrophysics.

We propose to use a different binning strategy based on the work of Gorski et al. (2005), which was also developed for binning astrophysical data and named HEALPix (Hierarchical Equal Area isoLatitude Pixelization). HEALPix has some appealing properties in the context of RTM angle gathers, namely: (i) it is based on equal-area bins, which renders amplitude corrections (such as the $1/\sin\theta$ correction) unnecessary; and (ii) it is adaptable to different acquisition configurations.

Gorski et al. (2005) define a binning procedure based on three integer parameters, noted as N_θ, N_ϕ and N_{side}. N_θ and N_ϕ define the so-called base configuration. In astrophysics, these are set to 3 and 4, respectively. Given the difference in the nature of the data sets used in geophysics, we have explored different values for these parameters, as varying them can be useful in adapting the binning to different acquisition geometries (e.g., hexagonal versus rectangular receiver grids). The third parameter N_{side} defines the level of refinement starting from the base configuration. The total number of pixels N_{pix} on the sphere for a given $(N_\theta, N_\phi, N_{side})$ is:

$$N_{pix} = N_\phi N_\theta N_{side}^2 \quad . \qquad (2)$$

Figure 1 provides a comparison between the spherical binning described here and a more traditional cylindrical binning. Bin parameters were chosen such that the total number of bins is roughly the same for both cases with incident angles limited to 60 degrees. Figures 1a and 1b show the projection of bin centers on the plane for the two cases. We observe that the HEALPix prescription provides a more distributed sampling of the sphere. Consequently, it is more suitable to a full-azimuth acquisition such as OBN. Figures 1c and 1d show the corresponding image gathers for all depths, sorted in incident angle/azimuth order. We have used the same binning definition for all depths.

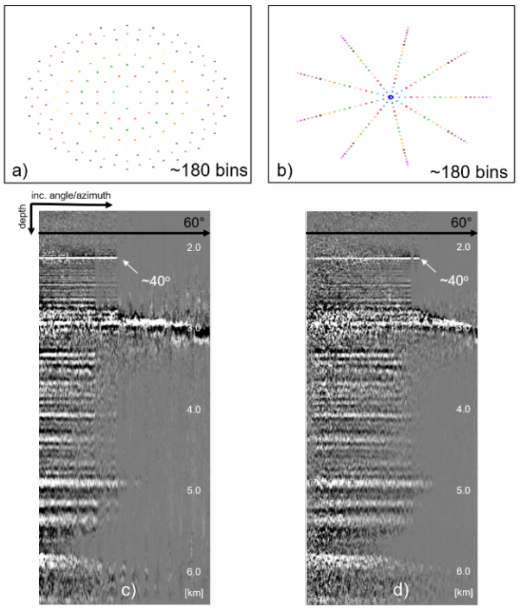

Figure 1: Projection of bin center positions for: (a) spherical binning, and (b) cylindrical binning. Corresponding angle "snail" gathers are shown in panels (c) and (d). In (b) we observe an over-sampling of the area around the pole while the far angle area is under-sampled. Because of this, the gather is considerably noisier in the cylindrical case. The HEALPix configuration used in (a) and (c) is $(N_\theta, N_\phi, N_{side}) = (7,6,4)$.

The binning procedure explained above defines a partition of the sphere, which can in turn be used to approximate integrals of functions defined on it. Specifically, one can define an interpolation formula that gives the value of that function at an arbitrary point on the sphere, given its value on the bin center positions. The interpolation is defined as follows (the derivation follows the lines of Ahrens and Beylkin, 2009):

$$f(\hat{r}_q) \approx \sum_p f(\hat{r}_p)\, t_{qp}\ ,\ t_{qp} = \frac{1}{N_{pix}} \sum_{l=0}^{l_{max}} (2l+1)\, P_l(\hat{r}_q \cdot \hat{r}_p)\ . \qquad (3)$$

The index q identifies an arbitrary position on the sphere given by $\hat{r}_q$, while the set $\{\hat{r}_p\}$ is defined on the HEALPix pixel positions. The interpolation matrix t_{qp} plays the role of the sinc interpolator on the sphere. It is defined as a sum of Legendre polynomials that depend only on the dot product

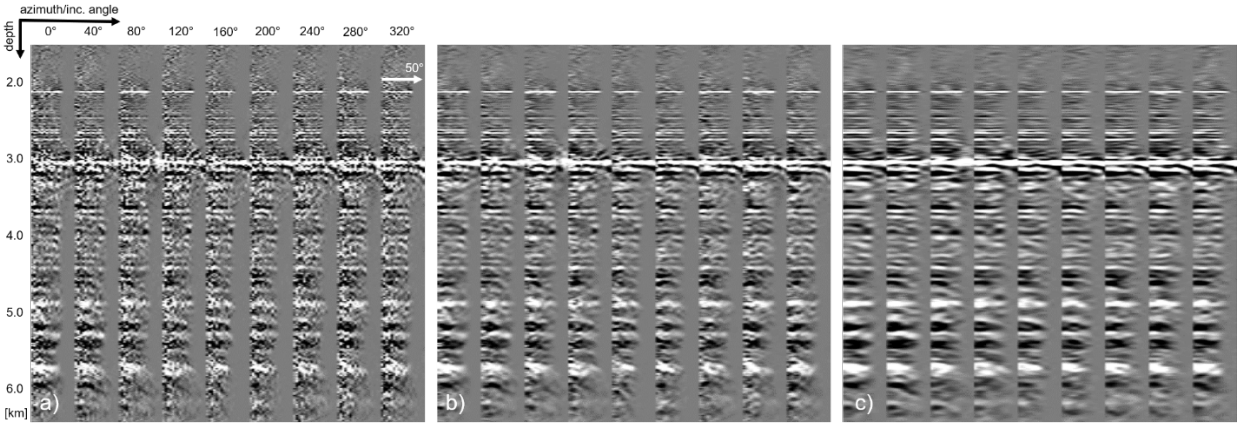

Figure 2: RTM 3D angle gathers at one image location: (a) cylindrical binning, (b) cylindrical binning with extrapolation method of Tang et al. (2011), and (c) spherical binning followed by interpolation back to cylindrical coordinates.

between $\hat{r}_q$ and the set of $\hat{r}_p$. The sum over l in the definition of t_{qp} is bounded by a parameter l_{max} that depends on the particular partition chosen. That is, it depends on $(N_\theta, N_\phi, N_{side})$, and it needs to be estimated. Tegmark (1996) suggests one such estimate:

$$l_{max} \approx \sqrt{3N_{pix}} \qquad (4)$$

In practice, we tested some percentages of that estimate for each binning configuration and data, which controls the level of smoothness of the image gather.

Figure 2c shows an image gather obtained after interpolation to cylindrical coordinates (sorted in azimuth/incident angle order), which is more suitable for azimuth-based post-processing. It contains nine azimuths with an increment of 40 degrees and incident angles with an increment of 3 degrees. Figure 2a shows the corresponding gather obtained through cylindrical binning. Figure 2b shows the result of the extrapolation method of Tang et al. (2011) applied to this gather. While it improves the image, some noise is still present, especially at near angles, which is resolved with the proposed spherical binning method. The image gathers in Figures 1 and 2 were obtained from the down-going wavefield of an OBN data set from the Santos Basin, offshore Brazil.

Data examples

We provide in this section additional analysis and quality controls. Figure 3 shows a stack and an image gather binned and interpolated to cylindrical coordinates. Sixteen azimuths are displayed, and incident angles have an increment of 3 degrees. The down-going wavefield was also used in this case. For this example, we used a HEALPix configuration of $(N_\theta, N_\phi, N_{side}) = (3,4,6)$.

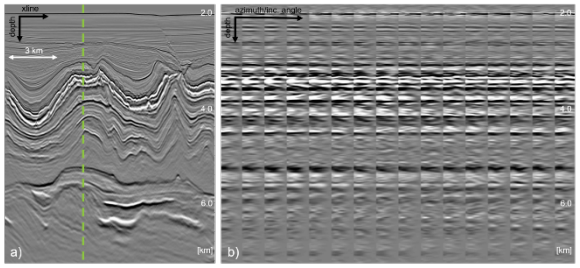

Figure 3: (a) Stack and (b) interpolated image gathers at location indicated by green dashed line.

To assess the amplitude behavior of the gathers, we performed an amplitude-versus-angle (AVA) analysis. We generated four partial stacks and compared the extracted amplitudes with synthetics generated at the base of salt (BOS) at three different well locations. The results are shown in Figure 4. We observe a good match with the synthetics, even though only a preliminary pre-conditioning, consisting of residual moveout and Radon, was applied. Note that we have used the interpolated gathers for this analysis in order to simplify the post-processing steps.

By comparing a near stack obtained from RTM angle gathers with the corresponding Kirchhoff near stack, we observe that the RTM image is cleaner overall with better event continuity, especially in the pre-salt (Figure 5). From the AVA analysis of RTM angle gathers and the comparison between the RTM near stack and Kirchhoff near stack, we can see that the RTM angle gather image extends the benefits of RTM to the prestack domain and can be used to replace

Kirchhoff gathers and partial stacks, which are the standard for AVA analysis.

We have not attempted to perform a moveout analysis (Biondi and Symes, 2004) on this data set. This is partly because confidence in the velocity for this data set was high, given that it was obtained through FWI (remember this is one of the main reasons for using OBN data in the first place). However, MVA on this data set could still be useful, and we leave this for further investigation.

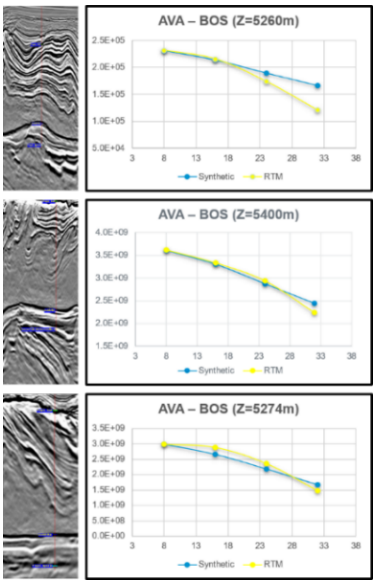

Figure 4: AVA extracted at the base of salt (BOS) at three different well locations, using four partial stacks and a preliminary pre-conditioning. RTM curves show a good agreement with the generated synthetics. Angle ranges of 3-13, 11-21, 19-29 and 27-37 were used to generate the partial stacks.

Before we conclude, we would like to close this section with a couple of remarks. First, it is important to remember that the new data sampling proposed here is just one of the many challenges faced when constructing angle gathers. Regarding the second class of algorithms mentioned before, they are all limited by the complexity of the wavefields, which in turn affects how the angles are estimated before the image is finally binned. They are also sensitive to aliasing in the wavefields, and any errors in this estimation will introduce noise in the RTM images. Second, a constant bin definition was used at all depths in the examples. However, a variable depth definition is possible. In severe cases where different bin definitions should be used, e.g., in the presence of a very strong velocity contrast, a hybrid approach combined with Tang et al. (2011) could be used. In this case, the extrapolation filter would be only depth dependent and applied on top of the binned data.

Conclusions

We presented a method for sampling the reflection energy used for constructing RTM 3D angle gathers. The approach is based on the work of Gorski et al. (2005), which was first introduced for binning astrophysical data. Next, we applied the method to OBN data from the Santos Basin, offshore Brazil and compared the results with those obtained through standard cylindrical binning and the extrapolation method of Tang et al. (2011). These results showed a significant improvement, especially at near angles, coming from a better sampling of these angles, combined with the fact that no amplitude correction had to be applied. We further analyzed the results by performing an AVA analysis at three different well locations, showing consistent amplitude behavior to synthetics generated at those positions. Finally, we have compared prestack images with those obtained by Kirchhoff migration, showing the benefits of reduced migration noise and improved continuity overall.

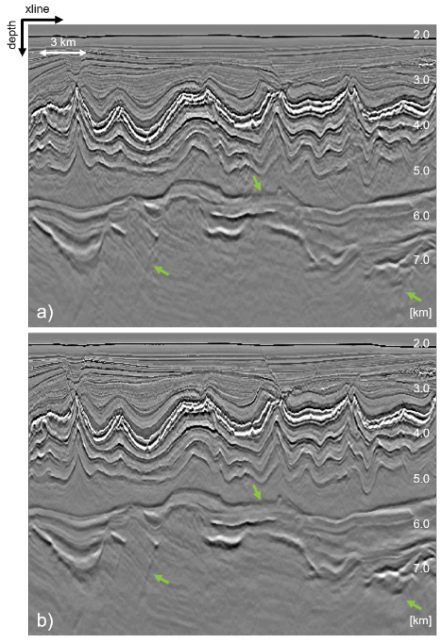

Figure 5: Near stack comparison for: (a) Kirchhoff and (b) RTM 3D angle gathers. The Kirchhoff image is filtered to the maximum frequency of the RTM.

Acknowledgments

We thank Petrobras and CGG for the permission to publish this work. We also thank Omar Roldan for pointing to the HEALPix paper, Andrei Alhadeff for help with the development, Samanta Bortoni for performing the AVA analysis, Ping Wang and Adel Khalil for useful suggestions, and Carlos Costa and Shannon Basile for revising the manuscript.

References

Ahrens, C., and G. Beylkin, 2009, Rotationally invariant quadratures for the sphere: Proceedings of the Royal Society A: Mathematical, Physical and Engineering Sciences, **465**, 3103–3125, doi: https://doi.org/10.1098/rspa.2009.0104.

Biondi, B., and W. W. Symes, 2004, Angle-domain common-image gathers for migration velocity analysis by wavefield- continuation imaging: Geophysics, **69**, no. 5, 1283–1298, doi: https://doi.org/10.1190/1.1801945.

Bunting, T., and J. Moses, 2016, The transformation of seabed seismic: First Break, **34**, 59–64, doi: https://doi.org/10.3997/1365-2397.34.11.87116.

Docherty, P. C., and W. A. Schneider Jr., 2016, Angle gathers and images from sparse OBN data: 78th Conference and Exhibition, EAGE, Extended Abstracts, We STZ1 08, doi: https://doi.org/10.3997/2214-4609.201601243.

Fomel, S., 2004, Theory of 3-D angle gathers in wave-equation imaging: 74th Annual International Meeting, SEG, Expanded Abstracts, 1053–1056, doi: https://doi.org/10.1190/1.1851067.

Gorski, K. M., E. Hivon, A. J. Banday, B. D. Wandelt, F. K. Hansen, M. Reinecke, and M. Bartelmann, 2005, HEALPix: A framework for high-resolution discretization and fast analysis of data distributed on the sphere: The Astrophysical Journal, **622**, 759–771, doi: https://doi.org/10.1086/427976.

Tang, B., S. Xu, and Y. Zhang, 2011, Aliasing in RTM 3D angle gathers: 81st Annual International Meeting, SEG, Expanded Abstracts, 3310–3314, doi: https://doi.org/10.1190/1.3627885.

Tegmark, M., 1996, An icosahedron-based method for pixelizing the celestial sphere: The Astrophysical Journal, **470**, L81–L84, doi: https://doi.org/10.1086/310310.

Tura, A., C. Hanitzsch, and H. Calandra, 1998, 3-D AVO migration/inversion of field data: The Leading Edge, **17**, 1578–1578, doi: https://doi.org/10.1190/1.1437898.

Vyas, M., D. Nichols, and E. Mobley, 2011, Efficient RTM angle gathers using source directions: 81st Annual International Meeting, SEG, Expanded Abstracts, 3104–3108, doi: https://doi.org/10.1190/1.3627840.

Xu, S., H. Chauris, G. Lambaré, and M. Noble, 2001, Common-angle migration: A strategy for imaging complex media: Geophysics, **66**, no. 6, 1877–1894, doi: https://doi.org/10.1190/1.1487131.

Xu, S., Y. Zhang, and B. Tang, 2011, 3D angle gathers from reverse time migration: Geophysics, **76**, no. 2, S77–S92, doi: https://doi.org/10.1190/1.3536527.

Yoon, K., and K. J. Marfurt, 2006, Reverse-time migration using the Poynting vector: Exploration Geophysics, **37**, 102–107, doi: https://doi.org/10.1071/EG06102.